PHYSICAL REVIEW D **89,** 074051 (2014)

Dipole model analysis of high precision HERA data

A. Luszczak[1] and H. Kowalski[2]
[1]*Tadeusz Kościuszko Cracow University of Technology, 30-084 Cracow, Poland*
[2]*Deutsches Elektronen-Synchrotron DESY, D-22607 Hamburg, Germany*
(Received 14 February 2014; published 30 April 2014)

We analyze, within a dipole model, the inclusive deep inelastic scattering cross section data, obtained from the combination of the measurements of the H1 and ZEUS experiments performed at the HERA collider. We show that these high precision data are very well described within the dipole model framework, which is complemented with valence quark structure functions. We discuss the properties of the gluon density obtained in this way.

DOI: 10.1103/PhysRevD.89.074051 PACS numbers: 13.60.Hb, 12.38.Bx, 13.85.Ni

I. INTRODUCTION

Many investigations have shown that HERA inclusive and diffractive deep inelastic scattering (DIS) cross sections are very well described by the dipole models [1–4]. Interest in the dipole description emerges from the fact that the dipole picture provides a natural description of QCD reaction in the low x region. Due to the optical theorem, dipole models allow a simultaneous description of many different physics reactions, like inclusive DIS processes, inclusive diffractive processes, exclusive J/ψ, ρ, ϕ production, diffractive jet production, or diffractive and non-diffractive charm production. In the dipole picture, all these processes are determined by the same, universal, gluon density [5–9].

In the era of the LHC, the precise knowledge of gluon density is very important because the QCD-evolved gluon density determines the cross sections of most relevant physics processes, e.g. Higgs boson production. Any significant deviation of the predicted cross section from their standard model value could be a sign of new physics.

The validity of the dipole approach was experimentally established, a decade ago, by a comparison of the dipole predictions with HERA F_2 and diffractive data in the low x region [1,2]. In the meantime, the precision of data obtained from HERA experiments increased substantially. The H1 and ZEUS experiments have combined their inclusive DIS cross sections which led to a substantial reduction of systematic measurement errors (due to cross calibration) and to an increase of precision of the combined data by about a factor of two [11]. In the same way the quality of the inclusive charm data was substantially improved [12]. Finally, recently, the exclusive J/ψ production was much more precisely measured [13]. All these reaction were used in the past to establish the dipole approach. It is therefore interesting to re-evaluate these reactions because the dipole picture provides a somewhat different approach to the gluon density than the usual parton density function (pdf) approach. In the usual pdf approach the gluon density contributes to F_2 mainly through the evolution of the sea quarks; the direct gluon contribution is only of the order of a few percent. On the other hand, in the dipole models the gluon density is directly connected to the sea quarks. In the pdf scheme the evolution is evaluated in the collinear approximation whereas the dipole approach uses the k_T factorization. Therefore, the quark mass effects are leading order (LO) effects in the dipole picture whereas they are next to leading order (NLO) in the collinear scheme.

The direct connection between the dipole production and gluon density is particularly clearly seen in the exclusive J/ψ production, which was therefore proposed as a testing ground of the properties of the gluon density [14,15]. Presently, the exclusive J/ψ production is precisely measured in heavy ion collisions at the RHIC and LHC. These measurements combined with their dipole analysis can become a new source of information about the gluonic structures of nuclei [16,17].

Another important application of the dipole description is the investigation of the gluonic high density states. These can be characterized by the degree by which a dipole is absorbed or multiply scattered in such states. The states with the highest gluon densities are produced today in the high energy heavy ion scattering at the RHIC and LHC. This is now a very lively field of saturation investigation [18,19].

The aim of this paper is to investigate the additional information which is contained in the combined HERA data [11]. The most precise data where obtained in the region of higher Q^2s [Q^2 from 3.5 to $O(1000)$ GeV^2], where the DGLAP evolution [10] is known to describe data very well. Therefore, in this investigation we employ the so-called BGK dipole model which uses the DGLAP evolution scheme.

This paper concentrates first on the *inclusive* DIS measurements in the low x region. Here, the contribution of the valence quarks is small, below 7%, and has therefore been neglected until now. However, the combined H1 and ZEUS HERA data [11] achieve a precision of about 2%, so the contribution of the valence quarks can no longer be neglected. The present paper addresses the question of to

what extent the contribution of the valence quarks and the dipoles are compatible with each other's. To do so we use the HERAFitter framework [20–24] which allows us to treat consistently QCD evolution together with the valence quark and dipoles contributions.

The paper is organized as follows: in Sec. II we recall the main properties of the dipole approach and review various models in order to motivate our choice. In Sec. III we discuss the results of fits and in Sec. IV we compare the fits with data. Section V contains the summary.

II. DIPOLE MODELS

In the dipole picture the deep inelastic scattering is viewed as a two stage process; first, the virtual photon fluctuates into a dipole, which consists of a quark-antiquark pair (or a $q\bar{q}g$ or $q\bar{q}gg\ldots$ system) and in the second stage the dipole interacts with the proton [25–32]. Dipole denotes a quasistable quantum mechanical state, which has a very long lifetime ($\approx 1/m_p x$) and a size r, which remains unchanged during scattering. The wave function Ψ determines the probability of finding a dipole of size r within a photon. This probability depends on the value of external Q^2 and the fraction of the photon momentum carried by the quarks forming the dipole, z. Neglecting the z dependence, in a very rough approximation, $Q^2 \sim 1/r^2$.

The scattering amplitude is a product of the virtual photon wave function, Ψ, with the dipole cross section, $\sigma_{\rm dip}$, which determines a probability of the dipole-proton scattering. Thus, within the dipole formulation of the $\gamma^* p$ scattering,

$$\sigma_{T,L}^{\gamma^* p}(x,Q^2) = \int d^2r \int dz \Psi^*_{T,L}(Q,r,z)\sigma_{\rm dip}(x,r)\Psi_{T,L}(Q,r,z), \tag{2.1}$$

where T, L denotes the virtual photon polarization and $\sigma_{T,L}^{\gamma^* p}$ the total inclusive DIS cross section.

Several dipole models have been developed to test various aspects of the data: [1–3,29,30] and [4,25–28,31–34]. They vary due to different assumptions made about the physical behavior of dipole cross sections. In the following we will shortly review some of them and motivate the choice of the model used for the present investigation.

A. GBW model

The dipole model became an important tool in investigations of deep inelastic scattering due to the initial observation of Golec-Biernat and Wüesthoff (GBW) [1], that a simple ansatz for the dipole cross section was able to simultaneously describe the total inclusive and diffractive cross sections.

In the GBW model the dipole-proton cross section $\sigma_{\rm dip}$ is given by

$$\sigma_{\rm dip}(x,r^2) = \sigma_0\left(1-\exp\left[-\frac{r^2}{4R_0^2(x)}\right]\right), \tag{2.2}$$

where r corresponds to the transverse separation between the quark and the antiquark, and R_0^2 is an x dependent scale parameter which has a meaning of saturation radius, $R_0^2(x) = (x/x_0)^{\lambda_{\rm GBW}}$. The free fitted parameters are the cross section normalization, σ_0, as well as x_0 and $\lambda_{\rm GBW}$. In this model saturation is taken into account in the eikonal approximation and the saturation radius is intimately related to the gluon density in the transverse plane; see below. The exponent $\lambda_{\rm GBW}$ determines the growth of the total and diffractive cross section with decreasing x. For dipole sizes which are large in comparison to the saturation radius, R_0, the dipole cross section saturates by approaching a constant value σ_0, i.e. saturation damps the growth of the gluon density at low x.

The GBW model provided a good description of data from medium Q^2 values (≈ 30 GeV^2) down to low Q^2 (≈ 0.1 GeV^2). Despite its success and its appealing simplicity, the model has some shortcomings; in particular, it describes the QCD evolution by a simple x dependence, $\sim(1/x)^{\lambda}_{\rm BGW}$, i.e. the Q^2 dependence of the cross section evolution is solely induced by the saturation effects. Therefore, it does not match with DGLAP QCD evolution, which is known to describe data very well from $Q^2 \approx 4$ GeV^2 to very large $Q^2 \approx 10000$ GeV^2.

B. BGK model

The evolution ansatz of the GBW model was improved in the model proposed by Bartels, Golec-Biernat, and Kowalski (BGK) [2] by taking into account the DGLAP evolution of the gluon density in an explicit way. The model preserves the GBW eikonal approximation to saturation and thus the dipole cross section is given by

$$\sigma_{\rm dip}(x,r^2) = \sigma_0\left(1-\exp\left[-\frac{\pi^2 r^2 \alpha_s(\mu^2) x g(x,\mu^2)}{3\sigma_0}\right]\right). \tag{2.3}$$

The evolution scale μ^2 is connected to the size of the dipole by $\mu^2 = C/r^2 + \mu_0^2$. This assumption allows us to consistently treat the contributions of large dipols without making the strong coupling constant, $\alpha_s(\mu^2)$, unphysically large.

The gluon density, which is parametrized at the starting scale μ_0^2, is evolved to larger scales, μ^2, using LO or NLO DGLAP evolution. We consider here three forms of the gluon density:

TABLE I. BGK NLO fit with valence quarks for σ_r for H1 ZEUS-NC-(e + p) and H1 ZEUS-NC-(e − p) data [11] in the range $Q^2 \geq 3.5$ GeV^2 and $x \leq 0.01$. *Soft gluon*.

No.	Q_0^2 [GeV^2]	σ_0	A_g	λ_g	C_g	C	Np	χ^2	χ^2/Np
1	1.1	143.14	1.605	−0.056	5.884	4.0	201	198.17	0.986
3	1.3	123.18	1.589	−0.094	6.937	4.0	201	200.70	0.998
5	1.5	112.44	1.685	−0.109	8.124	4.0	201	202.26	1.006
7	1.7	97.91	1.603	−0.137	8.849	4.0	201	203.55	1.013
9	1.9	90.98	1.624	−0.149	9.696	4.0	201	202.18	1.006

(i) the *soft* ansatz, as used in the original BGK model,

$$xg(x,\mu_0^2) = A_g x^{-\lambda_g}(1-x)^{C_g}, \tag{2.4}$$

(ii) the *soft* + *hard* ansatz,

$$xg(x,\mu_0^2) = A_g x^{-\lambda_g}(1-x)^{C_g}(1+D_g x+E_g x^2) \tag{2.5}$$

(iii) and the *soft* + *negative* gluon,

$$xg(x,\mu_0^2) = A_g x^{-\lambda_g}(1-x)^{C_g} - A'_g x^{-\lambda'_g}(1-x)^{C'_g}. \tag{2.6}$$

The free parameters for this model are σ_0, μ_0^2 and the parameters for gluon A_g, λ_g, C_g or additionally D_g, E_g, or A'_g, λ'_g, C'_g. Their values are obtained by a fit to the data. The fit results were found to be independent on the parameter C, which was therefore fixed as $C = 4$ GeV^2, in agreement with the original BGK fits.

C. IIM model

Although we do not use the IMM (Iancu, Itacura and Mounier) model in this paper, we mention it here because it may better take into account the saturation effects than is the case in the BGK or GBW models. The last models use the eikonal approximation for saturation, whereas the IIM model uses a simplified version of the Balitsky-Kovchegov equation [35]. The explicit formula for $\sigma_{\rm dip}$ can be found in [3]. The model was compared with the recent H1 data in [37], where it was shown that it provides a good data description in the lower Q^2 range, $0.2 < Q^2 < 40$ GeV^2. We do not use this model because we concentrate here on the higher Q^2 data, whose precise description requires an equally precise transition to the DGLAP regime.

D. Dipole model with valence quarks

The dipole models are valid in the low x region where the valence quark contribution is small. Therefore, this contribution was usually neglected which was justified as long as the experimental errors were relatively large. Theoretically, it is very difficult to treat valence quarks inside the dipole framework because, until now, the dipole amplitudes have not been well defined in the region of high x. The problem may be solved, in future, by the analytic continuation of the dipole (or BFKL) amplitudes from the low x to the high x region [36]. However, for the purpose of this paper, we propose to take a heuristic approach and just add the valence quark contribution from the standard pdf fits to the dipole predictions. In this approach the dipole contribution plays a role of the sea quarks in the standard pdfs. This procedure is justified by the fact that the sea quarks contribution disappears at larger x. The HERAFitter project [21,22] is well suited for this purpose since the dipole model and the valence quarks contributions are a part of the same framework.

III. RESULTS FROM FITS

In this section we investigate how well the dipole model can describe the precise HERA data [11] which were obtained in the region of $Q^2 > 3.5$ GeV^2. Since the quality of data in the region of $Q^2 < 1$ GeV^2 was not improved until now, we concentrate here on the higher Q^2 region where the valence quark contribution becomes relevant.

A. Dipole fits with valence quarks

First, we show that it is possible to combine the dipole and valence quark contributions and obtain a good fit to the data. For the purpose of this investigation, we choose the BGK model because it uses the DGLAP evolution. The fits were performed within the HERAFitter framework, which uses the QCD evolution as implemented in QCDNUM [21–23]. The fit of the gluon density was performed within the RT heavy flavor (HF) scheme.[1] The results of the BGK fit, with valence quarks, are shown in Table I. The fit is performed in the low x range, $x < 0.01$, for various μ_0^2 values, using data of Ref. [11]. The value of μ_0^2 plays a role of the starting scale of the QCD evolution which is usually denoted by Q_0^2 in the pdf fits. N_p denotes the number of measured values of the reduced cross section, σ_r, which were used in the fit. The parameters σ_0 of the dipole model and the parameters for gluon A_g, λ_g, C_g are obtained from the fit at a given value of Q_0^2 (in GeV^2). The value of the parameter C was fixed, as explained above.

[1]We mention this for completeness because, within the dipole model, the results of such a fit are independent of the scheme.

TABLE II. HERAPDF NLO fit for σ_r for H1 ZEUS-NC-(e + p) and H1 ZEUS-NC-(e − p) data [11] in the range $Q^2 \geq 3.5$ and $x \leq 1.0$.

No.	Q_0^2 [GeV^2]	χ^2	Np	χ^2/Np
1	1.1	604.64	592	1.021
3	1.3	586.33	592	0.990
5	1.5	579.72	592	0.979
7	1.7	576.76	592	0.974
9	1.9	575.08	592	0.971

Table I shows that the BGK model with valence quarks taken from the usual HERAFPDF1.0 fit [21,22] is describing the precise HERA data very well for all Q_0^2 values. The fit quality improves slightly with diminishing Q_0^2. This could indicate that HERA data in the low range of $Q^2 \sim 3.5$ GeV^2 retain some sensitivity to the saturation effects. In the BGK model the saturation effects increase with decreasing Q_0^2 values.

In Table II we show results of the standard HERAPDF fits performed with 10 free parameters, as in the HERAPDF1.0 case, in RT HF scheme [21,22]. The slight difference between the HERAPDF and HERAPDF1.0 fit is due to the use of a somewhat different data sample and a slightly different Q^2 range, see table captions, to be as compatible as possible with the dipole fit. The HERAPDF fit uses the full x range to properly fix the contribution of valence quarks.

Table II shows a very good agreement with data of the standard pdf fit. The agreement is similar as in the dipole fits, if corrected for the number of points and the number of free parameter, which is $N_{\text{free}} = 10$ for the HERAPDF fit and $N_{\text{free}} = 4$ in the case of the BGK fit with the *soft* gluon assumption. In contrast to the dipole fits, the quality of the HERAPDF fit is deteriorating with decreasing Q_0^2 scale.

TABLE III. HERAPDF NLO fit for σ_r for H1 ZEUS-NC-(e + p) and H1 ZEUS-NC-(e − p) data [11] in the range $Q^2 \geq 8.5$ and $x \leq 1.0$.

No.	Q_0^2 [GeV^2]	χ^2	Np	χ^2/Np
1	1.1	472.52	550	0.859
3	1.3	469.80	550	0.854
5	1.5	469.06	550	0.853
7	1.7	468.67	550	0.852
9	1.9	468.34	550	0.852

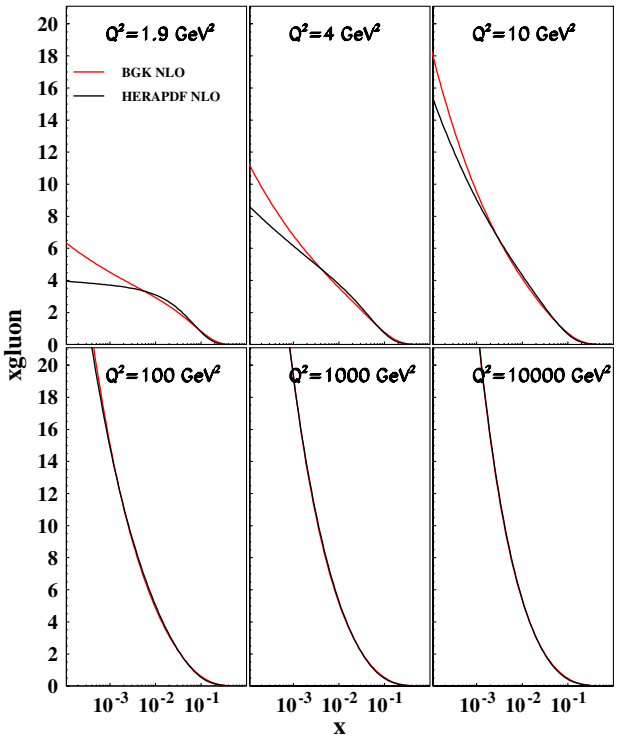

FIG. 1 (color online). Comparison between the gluon densities determined with the BGK dipole model (*soft*) and HERAPDF in NLO. The label xgluon on the vertical axis denotes $xg(x, Q^2)$.

Table III and IV show HERAPDF and BGK dipole fits in the higher Q^2 range, $Q^2 > 8.5$ GeV^2. The data sets used in the fit are indicated in the table captions. We see that the quality of fits clearly improves in the higher Q^2 region. In the case of the HERAPDF fit the χ^2/N_p improves from 0.97 to 0.85 and in the case of the BGK fit from ∼1.0 to 0.82. Moreover, the BGK fits do not show any dependence from the starting scale, Q_0^2. The HERAPDF fits do still show some slight deterioration with decreasing Q_0^2 but the effect is much smaller than that seen in Table II.

In Fig. 1 we show the gluon density obtained in the fits with valence quarks of Table I and compare it to the gluon density obtained in the HERAPDF fit. We see that the two gluon densities, at NLO, differ at smaller scales but then start to approach each other at higher scales. It is interesting

TABLE IV. Dipole model BGK NLO fit with valence quarks for σ_r for H1 ZEUS-NC-(e + p) and H1 ZEUS-NC-(e − p) data [11] in the range $Q^2 \geq 8.5$ and $x \leq 0.01$. NLO fit. *Soft gluon*.

No.	Q_0^2 [GeV^2]	σ_0	A_g	λ_g	C_g	C	Np	χ^2	χ^2/Np
1	1.1	91.60	2.227	−0.022	9.322	4.0	162	131.78	0.813
3	1.3	83.393	2.047	−0.069	10.019	4.0	162	132.10	0.815
5	1.5	77.121	1.969	−0.098	10.825	4.0	162	132.23	0.816
7	1.7	71.975	1.922	−0.120	11.538	4.0	162	132.88	0.820
9	1.9	69.128	1.897	−0.135	12.175	4.0	162	132.03	0.815

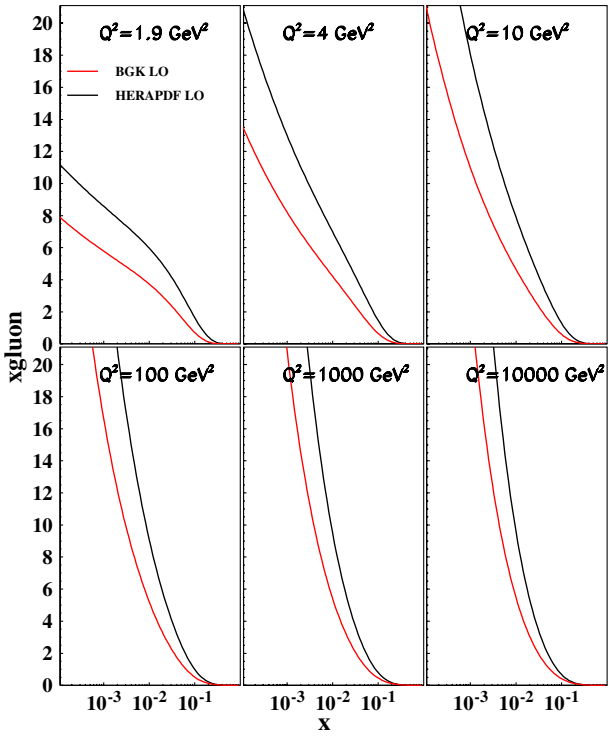

FIG. 2 (color online). Comparison between the gluon densities determined with the BGK dipole model (*soft*) and HERAPDF in NLO. The label xgluon on the vertical axis denotes $xg(x, Q^2)$.

to observe that the convergence of the two gluon densities is much slower in LO, Fig. 2.

B. Fits with alternative forms of the gluon density

In this section we investigate whether the more involved forms of the gluon density, Eq. (2.5) and Eq. (2.6), can improve the data description. In Table V and VI we show the fit results for the fits with *soft* + *hard* gluon of Eq. (2.5), in the lower $Q^2 > 3.5$ GeV^2 and higher $Q^2 > 8.5$ GeV^2 regions. We observe that the fit quality improves significantly by adding a "hard" component, $D_g x + E_g x$, to the classic soft gluon of Eq. (2.4). The value of χ^2 diminishes by about $\Delta\chi^2 \approx 20$ for $Q^2 > 3.5$ GeV^2 and by about $\Delta\chi^2 = 15$ for $Q^2 > 8.5$ GeV^2, which is a much larger drop than the increase of the parameter number (just by 2 units).

In Table VII we show the fit results for the fits with the *soft* + *negative* gluon of Eq. (2.6). The fit in the lower Q^2 range is not significantly improved by the addition of the negative gluon term. In the higher Q^2 range, $Q^2 > 8.5$ GeV^2, the fit improves somewhat, although not so clearly as in the hard case.

C. Fits without or with fitted valence quarks

To better understand the meaning of the fits which are using alternative forms of the gluon density, we also performed fits without valence quarks, and with valence quarks fitted to data. In Table VIII and Table IX we show fits performed without valence quarks for the *soft* and *soft* + *hard* forms of the gluon density in the region of $Q^2 > 3.5$ GeV^2.

The contributions of the valence quarks in the low x region are large enough to be able to determine them in this region only. In Table X we show an example of a fit with parameters of the valence quarks fitted to data together with the parameters of the gluon density. The fit is performed for $Q^2 > 3.5$ GeV^2, in the low x range, $x < 0.01$. In Table XI we give, for completeness, the parameters of the valence quarks determined in this way. Note that the fit with fitted valence quarks is better than the fit with fixed valence

TABLE V. Dipole model BGK NLO fit with valence quarks for σ_r for H1 ZEUS-NC-(e + p) and H1 ZEUS-NC-(e − p) data [11] in the range $Q^2 \geq 3.5$ and $x \leq 0.01$. *Soft* + *hard gluon*. $Np = 201$ and C = 4.0 GeV^2.

No.	Q_0^2 [GeV^2]	σ_0	A_g	λ_g	C_g	D_g	E_g	χ^2	χ^2/Np
1	1.1	217.09	1.976	−0.012	22.502	−35.364	1339.3	181.34	0.930
2	1.3	181.82	1.847	−0.059	21.597	−25.051	1030.3	180.80	0.927
3	1.5	165.17	1.871	−0.082	24.623	−23.630	1237.7	180.80	0.927
4	1.7	147.12	1.903	−0.099	26.720	−20.584	1310.2	181.70	0.932
5	1.9	132.26	1.948	−0.111	28.211	−18.008	1322.4	180.81	0.927

TABLE VI. Dipole model BGK NLO fit with valence quarks for σ_r for H1 ZEUS-NC-(e + p) and H1 ZEUS-NC-(e − p) data [11] in the range $Q^2 \geq 8.5$ and $x \leq 0.01$. *Soft* + *hard gluon*. $Np = 162$ and $C = 4.0$ GeV^2.

No	Q_0^2 [GeV^2]	σ_0	A_g	λ_g	C_g	D_g	E_g	χ^2	χ^2/Np
1	1.1	254.97	2.524	−0.027	24.857	−46.523	1639.8	117.34	0.752
2	1.3	154.25	2.171	−0.041	13.728	−20.261	340.97	121.79	0.781
3	1.5	292.89	2.358	−0.034	31.168	−50.312	2585.8	115.51	0.740
4	1.7	221.52	2.483	−0.051	34.010	−44.156	2630.6	115.78	0.742
5	1.9	174.46	2.490	−0.070	35.347	−37.706	2499.7	116.18	0.745

TABLE VII. Dipole model BGK NLO fit with valence quarks for σ_r for H1 ZEUS-NC-(e + p) and H1 ZEUS-NC-(e − p) data [11]. *Soft + negative gluon*. $C = 4.0$ GeV^2, $N_p = 201$ for $Q^2 > 3.5$ GeV^2 and $N_p = 162$ for $Q^2 > 8.5$ GeV^2.

Q_0^2 [GeV^2]	Q^2 [GeV^2]	σ_0	A_g	λ_g	C_g	A'_g	B'_g	C'_g	χ^2	χ^2/Np
1.9	3.5	115.09	0.874	−0.253	3.669	−0.014	−0.606	25.0	200.49	1.028
1.9	8.5	111.94	0.799	−0.290	3.922	0.020	−0.642	25.0	119.48	0.766

TABLE VIII. Dipole model BGK NLO fit without valence quarks for σ_r for H1 ZEUS-NC-(e + p) and H1 ZEUS-NC-(e − p) data [11] in the range $Q^2 \geq 3.5$ and $x \leq 0.01$. *Soft gluon*. $C = 4.0$ GeV^2 and $Np = 201$.

No	Q_0^2 [GeV^2]	Q^2 [GeV^2]	σ_0	A_g	λ_g	C_g	χ^2	χ^2/Np
1	1.9	3.5	115.09	2.038	−0.097	4.969	197.83	1.004

TABLE IX. Dipole model BGK fit without valence quarks for σ_r for H1 ZEUS-NC-(e + p) and H1 ZEUS-NC-(e − p) data [11] in the range $Q^2 \geq 3.5$ and $x \leq 0.01$. NLO fit. *Soft + hard gluon*. $C = 4.0$ GeV^2 and $Np = 201$.

No.	Q_0^2 [GeV^2]	Q^2 [GeV^2]	σ_0	A_g	λ_g	C_g	D_g	E_g	χ^2	χ^2/Np
1	1.9	3.5	119.18	1.970	−0.104	5.001	3.347	−19.340	196.26	1.006

TABLE X. Dipole model BGK fit with valence quarks fitted for σ_r for H1 ZEUS-NC-(e + p) and H1 ZEUS-NC-(e − p) data [11] in the range $Q^2 \geq 3.5$ and $x \leq 0.01$. NLO fit. *Soft gluon*. $C = 4.0$ GeV^2 and $Np = 201$.

No.	Q_0^2	Q^2	σ_0	A_g	λ_g	C_g	χ^2	χ^2/Np
1	1.9	3.5	88.040	1.766	−0.115	6.747	182.89	0.978

TABLE XI. Parameters for valence quarks from the dipole model BGK fit with valence quarks fitted for σ_r for H1 ZEUS-NC-(e + p) and H1 ZEUS-NC-(e − p) data [11] in the range $Q^2 \geq 3.5$ and $x \leq 0.01$. NLO fit. *Soft gluon*. Parameter $cBGK = 4.0$, $Np = 201$.

No.	*Auv*	*Buv*	*Cuv*	*Euv*	*Adv*	*Cdv*	*CUbar*	*ADbar*	*BDbar*	*CDbar*
1	3.717	0.665	4.652	9.694	2.189	4.291	2.582	0.100	−0.165	2.405

quarks of Table I and it is also better than the fit without valence quarks, Table VIII.

Figure 3 shows the comparison between the NLO gluon densities determined with the *soft* and *soft + hard assumptions*. The *soft* gluon density is taken from the fit of Table I. The *soft + hard* gluon density shown on the left-hand side of Fig. 3 is taken from the fit of Table V and was obtained with the fixed valence quark contribution. The right-hand side of this figure shows the *soft + hard* gluon density obtained from the fit of Table X. Here, the contribution of valence quarks is fitted to data together with the gluon density. Both fits, of Table V and Table X, have a very similar quality. The form of gluon densities differs, however, at lower scales in the high x region; the one with the fixed valence quarks shows a clear enhancement around $x \approx 0.1$, whereas the other shows no enhancement and has a form similar to the *soft* case. In all fits which we performed, the enhancement in the *soft + hard* gluon density fitted with the fixed valence quarks was always present, independently of the Q^2 cut or the LO or NLO QCD evolution. This enhancement disappears, however, when the valence quark contribution is fitted. Therefore, we do not attribute a physical meaning to this enhancement, especially that it is in the region which is not directly tested by data and that it contributes only to the low x region through the QCD evolution. Nevertheless, its existence emphasizes the necessity of a full fit to the data, i.e. of a fit in which the gluon density is fitted *together* with the valence quarks.

IV. COMPARISON WITH HERA DATA

In Fig. 4 we show a comparison of the dipole BGK fit with the HERA reduced cross section data. Figure 4 shows an excellent agreement of the fit with data. In Fig. 5 we show a comparison of F_l structure function obtained from the dipole BGK fit with H1 data [37] alone (i.e. not combined). In both figures we use the BGK fit of Table I, with $Q_0^2 = 1.9$ GeV^2. We note that a similar comparison of various dipole models with these H1 data, in the range $0.2 < Q^2 < 120$ GeV^2, was also made recently in [37] and [38,39].

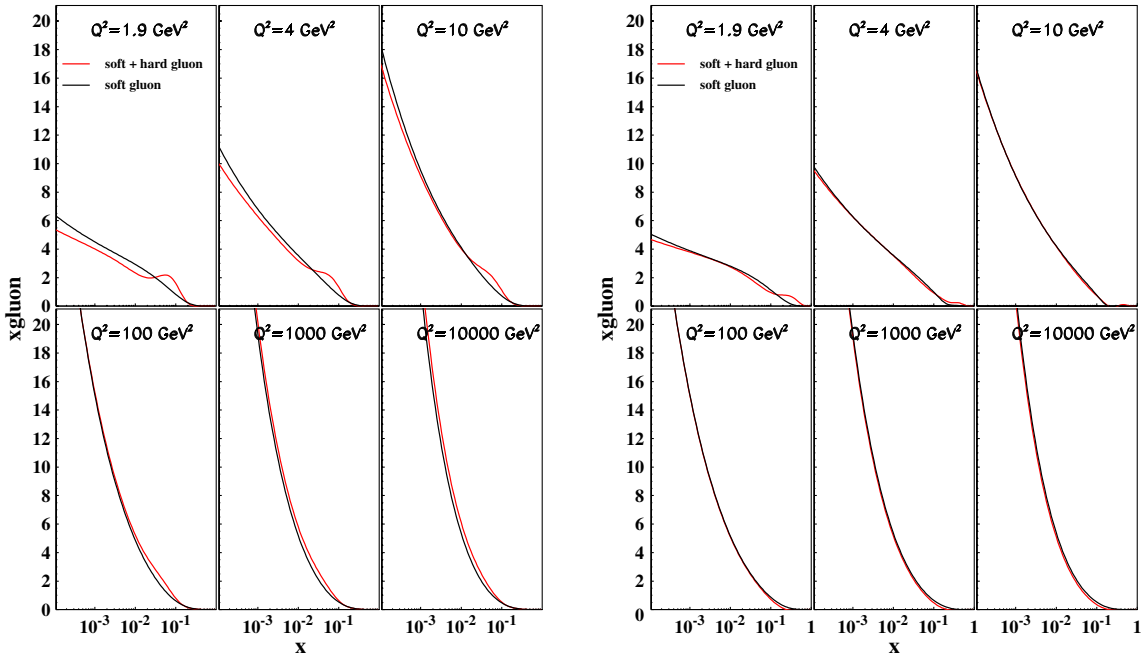

FIG. 3 (color online). Comparison between the NLO gluon densities determined with the *soft* and *soft + hard* assumptions. The left-hand side shows the gluon distribution functions determined with the fixed valence quark contribution. The right-hand side shows the gluon distribution functions determined with the contribution of valence quarks fitted to data in the $x < 0.01$ region. The label xgluon on the vertical axis denotes $xg(x, Q^2)$.

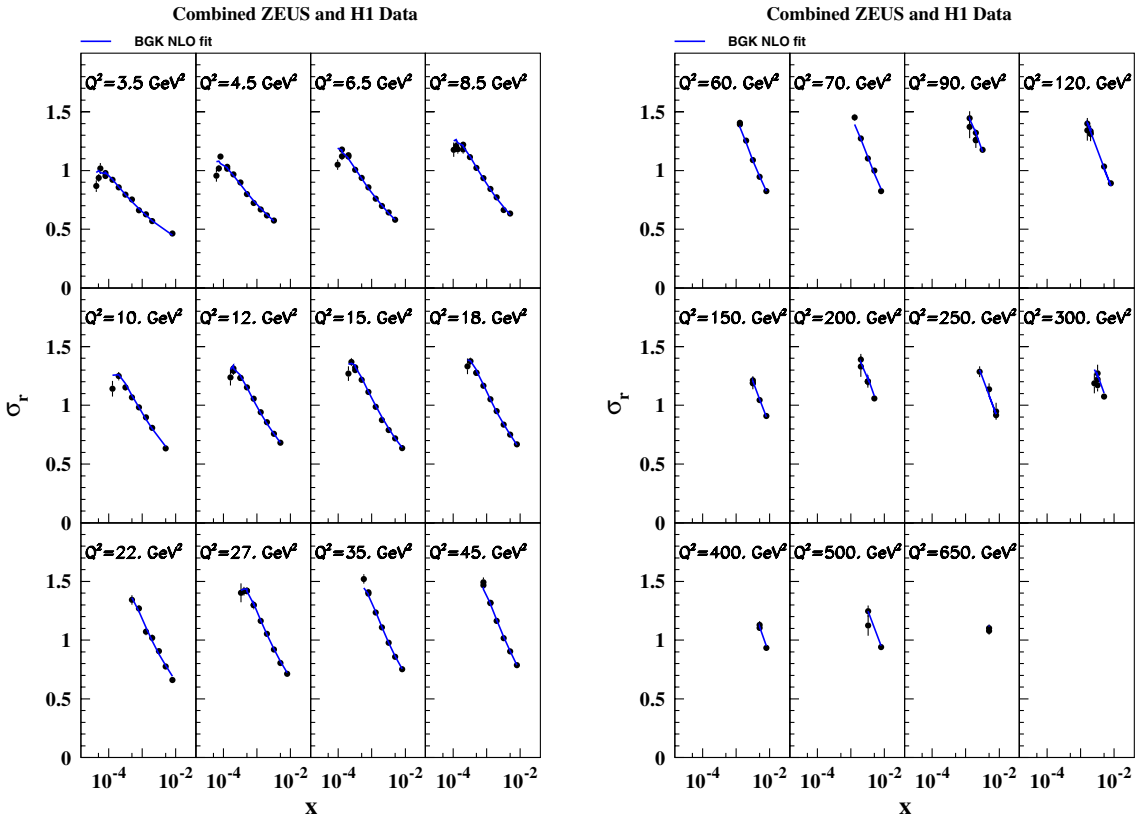

FIG. 4 (color online). Comparison of the dipole BGK fit of Table I with the reduced cross sections of the combined HERA data [11].

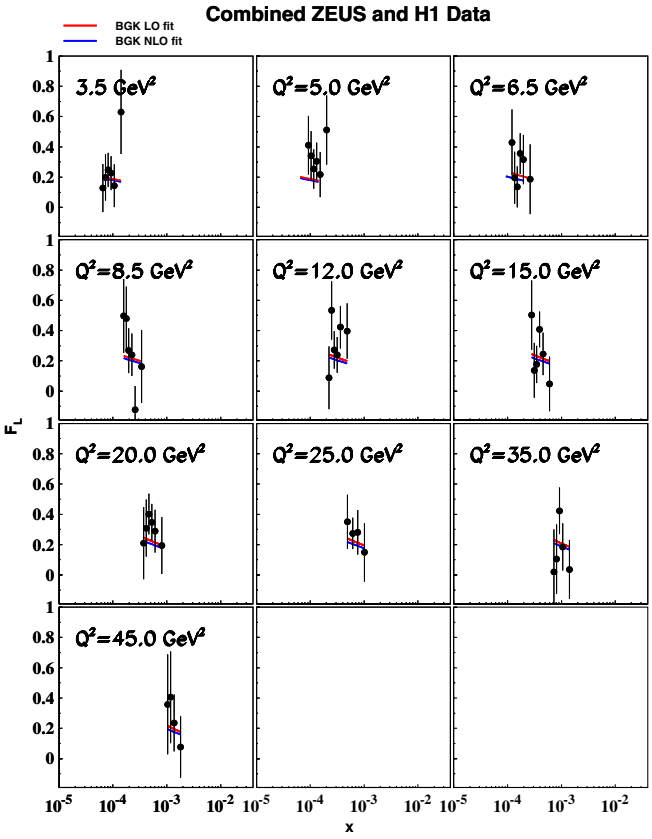

FIG. 5 (color online). Comparison of the F_l structure function obtained from the dipole BGK fit of Table I with H1 HERA data [37].

V. SUMMARY

We have shown that the k_T factorized, DGLAP evolved gluon density, evaluated within the BGK model, describes the combined, precise HERA data in the low x region very well. The valence quark contribution added to the dipole model improves the fit significantly. Therefore, for precise dipole evaluations the gluon contribution should be complemented by valence quarks.

The resulting gluon density obtained from fits with fitted valence quarks could be used for the prediction of LHC cross sections, provided that the dipole amplitude, which is now only well defined in the low x region, can be analytically continued to the high x region [36].

As a byproduct of this investigation we observe that the fits of all dipole and pdf types improve significantly when the Q^2 cut on data is increased from $Q^2 > 3.5$ to $Q^2 > 8.5$ GeV^2. We have checked this with the dipole model with quarks and without quarks, with various forms of the gluon density, as well as with the standard HERAPDF1.0 fit. The persistence of this effect indicates some shortcomings of the theoretical description; it could be due to the lack of higher order QCD corrections or to saturation effects. We note that the higher order corrections diminish logarithmically with increasing Q^2 whereas the saturation effects diminish like a power of Q^2, or faster.[2] In our view, the relatively fast change of χ^2/N_p with the increased Q^2 cut indicates that the effect is due to saturation, at least to a large extent. In this way, the increase of precision in HERA data offers a novel testing ground for a saturation study in the well measured region above $Q^2 > 3.5$ GeV^2. The study of this type may become very interesting when, in the near future, the combined HERA I and HERA II data, with yet further increased precision, is published.

ACKNOWLEDGMENTS

We thank P. Belov, A. Glazov, R. Placakyte and Voica Radescu for the introduction to the HERAFitter project and for various help with solving problems. We also thank J. Bartels and D. Ross for reading the manuscript and for useful comments.

[2]The degree of saturation is characterized by the size of the dipole, r_S, which, at a given x, starts to interact multiple times (in about 60% of cases). We recall that the saturation scale, $Q_S^2 = 2/r_S^2$, was determined at HERA as 0.5 GeV^2 at $x = 10^{-3}$ and as about 1 GeV^2 at $x = 10^{-4}$ [8]. Therefore, to avoid multiple scattering of dipoles, the Q^2 cut should be by about a factor of 10 higher than the saturation scale.

[1] K. Golec-Biernat and M. Wusthoff, Phys. Rev. D **59**, 014017 (1998); K. Golec-Biernat and M. Wusthoff, Phys. Rev. D **60**, 114023 (1999).
[2] J. Bartels, K. Golec-Biernat, and H. Kowalski, Phys. Rev. D **66**, 014001 (2002).
[3] E. Iancu, K. Itakura, and S. Munier, Phys. Lett. B **590**, 199 (2004).
[4] J. R. Forshaw, R. Sandapen, and G. Shaw, J. High Energy Phys. 11 (2006) 025.
[5] S. Munier, A. M. Stašto, and A. H. Mueller, Nucl. Phys. **B603**, 427 (2001).
[6] A. I. Shoshi, F. D. Steffen, and H. J. Pirner, Nucl. Phys. **A709**, 131 (2002).
[7] H. Kowalski and D. Teaney, Phys. Rev. D **68**, 114005 (2003).
[8] H. Kowalski, L. Motyka, and G. Watt, Phys. Rev. D **74**, 074016 (2006).
[9] G. Watt and H. Kowalski, Phys. Rev. D **78**, 014016 (2008).

[10] G. Altarelli and G. Parisi, Nucl. Phys. **B126**, 298 (1977); Yu. L. Dokshitzer, Sov. Phys. JETP **46**, 46 (1977); V. N. Gribov and L. N. Lipatov, Sov. J. Nucl. Phys. **15**, 438 (1972).
[11] F. D. Aaron *et al.* (H1 and ZEUS Collaborations), J. High Energy Phys. 01 (2010) 109.
[12] F. D. Aaron *et al.* (H1 and ZEUS Collaborations), Report No. DESY-12-172, 2012; F. D. Aaron *et al.*, Eur. Phys. J. C **73**, 2311 (2013).
[13] C. Alexa *et al.* (H1 Collaboration), Eur. Phys. J. C **73**, 2466 (2013).
[14] A. D. Martin, C. Nockles, M. G. Ryskin, and T. Teubner, Phys. Lett. B **662**, 252 (2008).
[15] S. P. Jones, A. D. Martin, M. G. Ryskin, and T. Teubner, J. High Energy Phys. 11 (2013) 085.
[16] A. Caldwell and H. Kowalski, Phys. Rev. C **81**, 025203 (2010).
[17] H. Kowalski, T. Lappi, and R. Venugopalan, Phys. Rev. Lett. **100**, 022303 (2008).
[18] Yuri V. Kovchegov, AIP Conf. Proc. **1520**, 3 (2013).
[19] R. Venugopalan (to be published).
[20] http://wiki-zeuthen.desy.de/HERAFitter/herafitter.org.
[21] F. D. Aaron *et al.* (H1 and ZEUS Collaborations), J. High Energy Phys. 01 (2010) 109.
[22] F. D. Aaron *et al.* (H1 Collaboration), Eur. Phys. J. C **64**, 561 (2009).
[23] M. Botje, Comput. Phys. Commun. **182**, 490 (2011).
[24] F. James and M. Roos (CERN), Comput. Phys. Commun. **10**, 343 (1975).
[25] N. N. Nikolaev and B. G. Zakharov, Z. Phys. C **49**, 607 (1991); N. N. Nikolaev and B. G. Zakharov, Z. Phys. C **53**, 331 (1992).
[26] J. Nemchik, N. N. Nikolaev, E. Predazzi, and B. G. Zakharov, Z. Phys. C **75**, 71 (1997).
[27] E. Gotsman, E. Levin, and U. Maor, Nucl. Phys. **B464**, 251 (1996).
[28] H. G. Dosch, T. Gousset, G. Kulzinger, and H. J. Pirner, Phys. Rev. D **55**, 2602 (1997).
[29] A. C. Caldwell and M. S. Soares, Nucl. Phys. **A696**, 125 (2001).
[30] J. R. Forshaw, R. Sandapen, and G. Shaw, Phys. Rev. D **69**, 094013 (2004).
[31] L. Frankfurt, M. Strikman, and C. Weiss, Annu. Rev. Nucl. Part. Sci. **55**, 403 (2005).
[32] H. Kowalski, T. Lappi, C. Marquet, and R. Venugopalan, Phys. Rev. C **78**, 045201 (2008).
[33] K. Golec-Biernat, Habilitation Thesis, Henryk Niewodniczanski Institute of Nuclear Physics [Institution Report No. 1877/PH, 2001 (unpublished)], http://www.ifj.edu.pl/publ/reports/2001/1877.pdf.
[34] L. Frankfurt, A. Radyushkin, and M. Strikman, Phys. Rev. D **55**, 98 (1997).
[35] I. Balitsky, Nucl. Phys. **B463**, 99 (1996).
[36] H. Kowalski, L. N. Lipatov, and D. A. Ross (to be published).
[37] F. D. Aaron *et al.* (H1 Collaboration), Eur. Phys. J. C **71**, 1579 (2011).
[38] P. Belov, Report No. DESY-THESIS-2013-017.
[39] A. H. Rezaeian, M. Siddikov, M. Van de Klundert, and R. Venugopalan, Phys. Rev. D **87**, 034002 (2013).